https://doi.org/10.5194/egusphere-2023-1975

More than one landslide per road kilometer – surveying and modeling mass movements along the Rishikesh-Joshimath (NH-7) highway, Uttarakhand, India

Jürgen Mey[1], Ravi Kumar Guntu[2], Alexander Plakias[1], Igo Silva de Almeida[1], Wolfgang Schwanghart[1]

[1]Institute of Environmental Science and Geography, University of Potsdam, Potsdam-Golm, 14476, Germany
[2]Department of Hydrology, IIT Roorkee, Roorkee, 247667, India

Correspondence to: Jürgen Mey (juemey@uni-potsdam.de)

10   **Abstract.** The rapidly expanding Himalayan road network connects rural mountainous regions. However, the fragility of the landscape and poor road construction practices lead to frequent mass movements along-side roads. In this study, we investigate fully or partially road-blocking landslides along the National Highway (NH-7) in Uttarakhand, India, between Rishikesh and Joshimath. Based on an inventory of >300 landslides along the ~250 km long corridor following exceptionally high rainfall during September and October, 2022, we identify the main controls on the spatial occurrence of mass-

15   movement events. Our analysis and modeling approach conceptualizes landslides as a network-attached spatial point pattern. We evaluate different gridded rainfall products and infer the controls on landslide occurrence using Bayesian analysis of an inhomogeneous Poisson process model. Our results reveal that slope, rainfall amounts, lithology and road widening are the main controls on landslide occurrence. The individual effects of aggregated lithozones are consistent with previous assessments of landslide susceptibilities of rock types in the Himalayas. Our model spatially predicts landslide occurrences

20   and can be adapted for other rainfall scenarios, and thus has potential applications for efficiently allocating efforts for road maintenance. To this end, our results highlight the vulnerability of the Himalayan road network to landslides. Climate change and increasing exposure along this pilgrimage route will likely exacerbate landslide risk along the NH-7 in the future.

Keywords: landslide inventory, road infrastructure, Himalayas, landslide risk, network-attached point pattern

25   **Statements and Declarations**

Competing interests: The authors declare that they have no conflict of interest.

1 Introduction

Roads are at the heart of the Himalayan transport infrastructure. They are vital for national and international trade and
30   passenger movement, and strategically important in border areas. India has improved and expanded its road network in mountainous states e.g. under the national Bharatmala Pariyojana ("Road to Prosperity") initiative, established in 2015. Key objectives of this highway development program are to improve the efficiency and connectivity of the transport

infrastructure and to provide road access to remote border regions and rural areas. Yet, in mountainous environments, roads are exposed to various degrading processes. Among these processes, mass movements particularly inflict severe structural

35   damage and heavily degrade road serviceability (Meyer et al., 2015). Traffic disruptions due to mass movements can have severe consequences, if they impede accessibility and compromise rescue operations during extreme events such as cloudbursts, floods and earthquakes. Ensuring accessibility and connectivity thus requires considerable maintenance efforts (Uniyal, 2021).

40   According to the National Crime Records Bureau (2022), 160 people died due to landsliding in Uttarakhand in the last four years. These figures exclude other extreme events like heavy rainfalls, floods or the 2021 Chamoli rock and ice avalanche with over 200 fatalities (Shugar et al., 2021). Several studies have addressed mass movements and their relation to transport infrastructure in the Indian and Nepal Himalayas. The studies range from purely phenomenological descriptions (e.g., Bartarya & Valdiya, 1989; Sarkar & Kanungo, 2006), to statistical (Das et al., 2012; Devkota et al., 2013; Sur et al., 2020)

45   and physically based modeling approaches (e.g., Kanungo et al., 2013; Prasad & Siddique, 2020). In fact, the space limitation in steep terrain often requires road construction to undercut slopes beyond their angle of repose, reducing slope stability and increasing landslide susceptibility (e.g., Barnard et al., 2001; Haigh & Rawat, 2011; Li et al., 2020). The increase in mass wasting due to road construction itself may be similar to the impact of a large earthquake (Tanyas et al. 2022). Therefore, particular attention has focused on detailed stability assessments of road cut slopes (e.g., Kundu et al.,

50   2016; Siddique et al., 2017; Siddique & Pradhan, 2018; Singh et al., 2014) and the development of appropriate remedial measures (e.g., Adhikari et al., 2020; Asthana & Khare, 2022; Koushik et al., 2016; Rawat et al., 2016), but fewer studies have attempted to predict the spatial occurrence of mass movements along roads. Knowledge about where and when landslides preferably detach is important for early warning but also for efficiently allocating efforts of road maintenance and slope enforcement (Haigh, 1984). Using data on occurrences of landslides, susceptibility studies aim to quantify the spatial

55   propensity of hillslopes to fail and to determine the controlling factors such as terrain attributes e.g., slope angle and aspect, and geo-environmental variables e.g., rainfall intensity and lithology.

In this study we carry out an analysis of road exposure to landsliding for a ~250 km long stretch of the National Highway 7 (NH-7) that connects the cities of Rishikesh and Joshimath, Uttarakhand, India (Fig.1). We conducted a detailed survey of

60   partially or fully road-blocking landslides along the road, following a period of intense rainfalls in September and October 2022. Limiting the inventory to road blocking landslides was required to cope with the overwhelming number of landslides and to ensure that we account for the landslides that detached most recently. In addition, construction works for road widening often stripped away the vegetation so that differentiating between actual, non-blocking landslides and excavated slopes was not straightforward. In contrast to previous studies, which focused on the spatial prediction of landslides in two

65   spatial dimensions, our analysis and modeling approach conceptualizes landslides as a network-attached spatial point pattern (Baddeley et al., 2021). The objective of this study is to test whether such a simplified approach would be particularly feasible to determine the inter-relationship between linear communication infrastructure and landslides. One of the critical covariates in our modeling approach is the spatial distribution of accumulated rainfall amounts. We thus evaluate different rainfall products. Finally, we infer the controls on landslide occurrence using Bayesian analysis of multivariate loglinear

70   models. We present our results and discuss uncertainties and potential shortcomings of our approach. We conclude with recommendations for refinement of the approach and further research avenues.

2 Study site

The NH-7 ascends from 400 m at Rishikesh to approximately 2000 m at Joshimath, crossing steep terrain with soil mantled slopes that range in inclination from 20° to 40°. Mean annual rainfall (1970–2019) varies from 1500–2000 mm around Rishikesh to 1000–1200 in Joshimath with 80–86 % and 60–70 % delivered by the Indian summer monsoon (June to September), respectively (Pai et al., 2014; Swarnkar et al., 2021). Air temperature in Rishikesh is always above freezing and ranges between 4 and 40 °C, whereas the temperature in Joshimath varies between -10 and 20 °C. This climatic gradient is reflected in a gradual change in vegetation. Accordingly, in the lower lying subtropical region dense deciduous forest dominates, which is replaced by a temperate broadleaf mixed forest and temperate shrub and grassland communities where forest has not been preserved.

The geological framework of the study area is largely determined by the ongoing Indo–Asian collision that causes crustal thickening and exhumation along large-scale detachment zones and thrust faults. Most of the study area lies within the Lesser Himalaya, between the Main Boundary Thrust in the south and the Main Central Thrust in the north, which are both splays of the root detachment, the Main Himalayan Thrust (Fig. 1). As the present-day India–Eurasia convergence is on the order of 36–40 mm yr^{-1} (e.g., Wang et al., 2001) and approximately half of this is accommodated within the Himalayas (e.g., Lavé & Avouac, 2000), the region is seismically active and bears the potential for large earthquakes (e.g., Kayal et al., 2003; Bollinger et al., 2014; Rajendran et al., 2017).

The highway runs perpendicular to the strike of the orogen and crosses rocks of the Lesser Himalayan Sequence (LHS) and the High Himalayan Crystalline (HHC) that represent the ancient passive Indian margin, and which are separated by the Main Central Thrust (MCT). The LHS is mainly composed of sedimentary and low-grade metasedimentary rocks; quartzite, shale, phyllites and slate with occasional limestone and dolomite, whereas the HHC is characterized by high-grade schist, gneiss and quartzite. These rocks feature a high density of discontinuities like faults, fractures and joints that are important seepage pathways. In locations, where the road cuts through weathered rocks and intersects with major faults, the hillslopes are particularly fragile (Prasad & Siddique, 2020).

During the week before we conducted our survey, almost the entire Indian north experienced a strong positive rainfall anomaly. The state of Uttarakhand registered a departure of 1040 % from the average. The districts of Tehri Garhwal, Pauri Garhwal, Rudraprayag and Chamoli, through which the NH-7 runs, recorded a weekly surplus of 419 %, 679 %, 218 % and 1855 %, respectively (https://mausam.imd.gov.in/imd_latest/contents/rainfall_statistics_2.php, supplementary data). Given that the mean monthly rainfall in October is around 35 mm, approximately three times the monthly average rainfall occurred in only one week, which is close to the rate that prevails during the monsoon.

The NH-7 is a lifeline for socioeconomic development, which is mainly based on agriculture, trade, tourism, mining and hydropower. Furthermore, the highway is vital for the Indian military to transport personnel and equipment to their outposts up to the Indian/Chinese-Tibetan border. During the pilgrimage season (May – Oct) more than one million people visit the holy shrines of Badrinath and Kedarnath using this highway. Moreover, as it follows the course of the Ganges and its tributary Alaknanda, the road passes the river confluences known as the five Prayags, namely Devprayag, Rudraprayag, Karnaprayag, Nandaprayag and Vishnuprayag (Fig. 1). In Hinduism, these confluences are considered sacred and attract pilgrims to bathe in the flows before worshiping the rivers. Finally, there are ten hydroelectric power plants within 20 km distance to the road and numerous more are planned or are under construction, highlighting the road's importance in terms of energy security and economic value.

3 Methods

Traveling to fieldwork in the Chamoli area on Oct 15, 2022, we recognized numerous, partially road-blocking landslides along the road. We recorded these landslides as road workers already began to clean the road from the debris, thus rapidly removing evidence of smaller landslides that detached in close vicinity to the road. We mapped landslides along the road both on our way towards Joshimath on Oct 15 and 16, as well as on our way back on Oct 18, 2022. We used handheld GPS devices to map the locations, at which landslides intersected with the road between Rishikesh and Joshimath, Uttarakhand (Fig. 1). We only mapped landslides with runouts affecting the road, thus partially or fully blocking it (Fig. 2). We considered partial blockages as those, where the emplaced deposits either substantially narrowed the road, or if debris crossed marginal road markings. Very small landslides with an area of less than ~10 m^2 were not considered. We checked each landslide location using Google Earth using the latest and historic imagery and classified each location as (1) new landslide, (2) road-blocking landslide visible before the Sep–Oct 2022 rainfall anomaly, and (3) reactivated landslide. We assigned the last category to those landslides where a slip surface and scar were well-identifiable in the imagery, prior to the observation period. This was not always straightforward since landslide scars cannot always be clearly distinguished from unvegetated engineered slopes and road widening. Note that by April 2023, Google has removed historic imagery of India prior to 2018 from the public domain, supposedly for reprocessing[1].

We conceptualize landslides along the road as a network-attached spatial point process. A spatial point process is a stochastic mechanism, which controls the spatial distribution of events or occurrences (Baddeley et al., 2015). As our mapped landslides are events that occur along the road – and only these have been mapped – these events are constrained to lie on a network of lines (Baddeley et al. 2021, Okabe et al. 2006). In our case, the network is rather simple as it consists of only one polyline, but we emphasize that our approach can be extended to more complicated network topologies.

We use the open-source MATLAB extension TopoToolbox (Schwanghart and Scherler, 2014) and its numerical object PPS (Schwanghart et al., 2021) to analyze, visualize, and model the density of landslides along the road. PPS has been designed to work with point patterns on stream networks, but it can be applied to dendritic, undirected networks of any kind. The numerical approach consists of a fine-pixel approximation which is controlled by the geometry of the digital elevation model (DEM), from which the data is retrieved. This means that the vector shape of the road is pixelated with the same geometry as the DEM (Schwanghart et al., 2021). We model landslide densities with an inhomogeneous Poisson process, which is described by its intensity function $\lambda(u)$ with u being the horizontal distance along the road. A common parametric model of the intensity is the loglinear model:

$$\lambda(u) = exp(\beta_0 + \beta X), \tag{1}$$

where X is a matrix of predictor variables (covariates), β_0 is an intercept and β is a vector of model parameters. A key property of the model is that the events are independent from each other. Spatial dependence of events can occur in different ways leading to clustering, i.e., points tend to occur close to other points, or inhibition, i.e., there is a characteristic distance or regularity in the spacing between the points. Spatial clustering of landslide events has previously been addressed by Lombardo et al. (2018, 2019) using a Cox Process model to emulate the latent spatial effects of unobserved variables, whereas inhibition can be observed, for example, in data where areal non-overlapping phenomena are represented as points (Evans, 2012; Schwanghart et al., 2021). At this stage, we will not include these potential second-order effects on the density of landslides, but we will investigate their possibility using the inhomogeneous K-function defined by Ang et al., (2012) once we have modeled first-order effects.

---

[1] https://www.thehindu.com/news/national/google-historical-satellite-imagery-disappears-for-india/article66834033.ece

We use the following candidate predictor variables in the loglinear model introduced above. First, we hypothesize that steep hillslopes gradients next to the road are more susceptible to mass wasting events. Therefore we calculate surface gradients, based on the Copernicus 30 m DEM (European Space Agency, 2021). We identify areas that lie right or left to the road, and which are higher than the road itself within a buffer zone of ~210 m (or 7 pixels). We then identify the nearest DEM pixels

160 and map the mean gradients of these nearest pixels to the road network. We chose 210 m (7 x spatial resolution of the DEM) to have sufficient pixels to obtain robust estimates of the slope. These values still vary greatly over short distances along the road and thus we smooth them using the algorithms (with smoothness penalty parameter K = 3.5) described by Schwanghart and Scherler (2017).

165 In addition to gradient, we hypothesize that rainfall patterns exert a strong influence on the occurrence of landslides. We chose five rainfall products (see Table 1) to comprehend spatial patterns of accumulated rainfall from January 1 to October 10, 2022. We extended the temporal range of the rainfall products beyond the Sep-Oct rainfall anomaly because of the limited temporal resolution of the historical high resolution Google Earth imagery, which impedes clear attribution of landslides to this event. We evaluated five different gridded rainfall products, of which IMD1 is solely taking into account

170 gauge-based measurements from a network of stations provided by the Indian Meteorological Department (Pai et al., 2014). Gauge measurements are merged with Integrated Multi-satellite Retrievals for Global Precipitation Measurement (IMERG) final run estimates in IMD2 (Mitra et al., 2009). MSWEP v2 is another merged product that incorporates reanalysis-based, gauge, and satellite-derived rainfall estimates (Beck et al., 2017). CHIRPS v2 provides a high-resolution record by combining gauge and satellite data from NOAA (National Oceanic and Atmospheric Administration) (Funk et al., 2015) and

175 the IMERG late run provides gridded multi-satellite precipitation estimates with quasi-Lagrangian time interpolation from NASA (National Aeronautics and Space Administration) (Huffman et al., 2014). We projected the geographic coordinates of the rainfall grids to UTM zone 44N and bilinearly resampled the data to the resolution of the DEM before extracting the values for each road pixel.

180 Next, we incorporate information about road widening by creating a logical mask that identifies the widened segments of the highway. Due to the lack of other data we use the map of Sati et al. (2011) that displays where road widening has been undertaken prior to the monsoon season of 2010. Our effort of compiling a more recent database of road widening using historic imagery from Google Earth was rendered impossible after most of the respective images were removed from the public archive in April 2023.

185

Finally, we obtained a digitized version of the lithology of Uttarakhand in the scale of 1:2M from the Geological Survey of India (2022). The data contains both stratigraphic as well as lithological information. Accordingly, the NH-7 crosses 34 different lithologies along the stretch from Rishikesh to Joshimath. To reduce the number of potential categories, we summarized and aggregated the lithological information into lithozones with less focus on the stratigraphic context. This

190 simplification resulted in five lithozones that are dominated by carbonate rocks (1), phyllite and shale (2), quartzite (3), quartzite and igneous rocks (4) and crystalline high grade metamorphic rocks (5). The reclassification is shown in Table 2. Again, we gridded this data and assigned corresponding lithozones to each road pixel.

We adopt a Bayesian strategy to infer and identify predictor variables using the function bayesloglinear of the PPS numerical

195 class (Schwanghart et al., 2021). The function provides an interface to bayesreg (Makalic and Schmidt, 2016), a MATLAB toolbox that enables efficient Bayesian modeling and regularization of high-dimensional data. We use a Bayesian lasso estimator with Laplace prior distributions for the regression coefficients. The sampling creates 1000 burnin samples before

calculating 1000 posterior samples. To avoid autocorrelation of the posterior samples, we use a level of thinning of five samples. To this end, we find that 1000 samples are sufficient to characterize the posterior distributions.

200

Finally, we evaluate the model based on the Receiver-Operating Characteristics (ROC) Area under the Curve (AUC) approach (e.g., Hanley and McNeil, 1982). We visualize the predictions and inspect and analyze spatial densities obtained from random realizations of the fitted inhomogeneous Poisson process model. Moreover, we evaluate the predictive performance of the model using a 5-fold cross-validation. In this approach, we subdivide the road into 15 km segments,

205 which are then randomly partitioned into 5 groups. The first group is used as test data while the remaining groups are used to train the model. This step is then repeated for each group and the performance summarized with the AUC. In addition, we test whether additional covariates provide opportunities for further improving the model. The selected attributes include terrain roughness and total curvature as well as land cover derived from the Copernicus Global Land Operations (CGLOPS-1, Moderate dynamic land cover 100 m, version 3) (Buchhorn et al., 2020), which we reclassify according to Table 3. We

210 investigate these models using a frequentist modeling approach (see PPS-function fitloglinear) and compare models with additional covariates with the Akaike Information Criterion (AIC, Akaike, 1974).

4 Results

We recorded 309 fully or partially road-blocking landslides along the 247 km long road between Rishikesh and Joshimath (Fig. 1) which amounts to an average landslide density of 1.25 landslides per km. The average nearest distance between

215 adjacent landslides is 315 m which demonstrates that the points are unevenly distributed along the road. A two-sample Kolmogorov-Smirnoff test between the road distance (uniform distribution between start and end of the surveyed road), and the road distances measured at the landslides rejects the null hypothesis with $p \approx 0$ that landslide locations follow a completely spatial random distribution. Yet not all field-mapped landslide occurrences can be attributed to the anomalously high rainfall period during September and October 2022. Visually inspecting the locations using Google Earth reveals that

220 21.4 % of the recorded landslides with road blockages existed before (Fig. 1). 17.8 % of the landslides were most likely reactivated by the excessive rainfall because they could not be identified to be road-blocking before the rainfall period. Most landslides (60.8 %) were not identifiable as such in the Google Earth imagery available for several dates before and including March 2022.

225 The spatial distribution and amounts of accumulated rainfall between January 1 and October 10 differ between the rainfall products (Fig. 3). Since independent measurements based on rain gauges are unavailable, we investigate the performance of the rainfall products to explain the spatial distribution of landslides. The approach uses the AIC to iteratively evaluate models including one of the rainfall products at a time, as well as hillslope gradient, lithozones, and road widening. AIC values vary between 2239 and 2258 with CHIRPS v2 having the lowest AIC. CHIRPS v2 correlates positively with landslide

230 density, whereas all other rainfall products show negative or no significant correlation (supplementary data). We thus use CHIRPS v2 in the development of the subsequent models. We emphasize that including different rainfall products in the model has no strong effect on the remaining model parameters that determine the influence of slope and lithozones and road widening. In other words, the choice of rainfall product does not affect our results and conclusions about the topographic and lithologic controls on landslide occurrence.

235

Bayesian loglinear modeling of the landslide density (Fig. 4, Fig. 5a, b) reveals a credible influence of the covariates rainfall (Fig. 5c), slope (Fig. 5d), lithozones (Fig. 5e) and road widening (Fig. 5f) (see Fig. 4 for posterior means and 95 % highest density intervals and Fig. 6 for individual effects). A Bayesian feature rank algorithm based on the absolute magnitude of the

parameters in each posterior sample (Makalic and Schmidt, 2011), ranks slope as the top covariate in terms of explanatory
power, followed by rainfall, road widening and lithozones. Among the lithozones, zones 4 and 2 stand out as important
categories improving the explanatory power of the model. The individual effects of the covariates reveal a positive influence
of rainfall and slope on landslides (Fig. 6a, b). Predictions of landslides densities in lithozone 4 are credibly lower than in
lithozone 2 (Fig. 6c). Also, our model suggests that road widening affects the density of landslides. Corrected for the
influence of other parameters, average densities are twice as high in widened road sections (Fig. 6d). The spatial pattern of
predicted landslide density (Fig. 5g) is consistent with observed spatial density variations, but the higher variability reflects
the importance of slope as a predictor variable.

The AUC is an aggregated metric for a point pattern model across thresholds and ranges between 0.5 and 1, with values
close to 1 indicating high performance of a model. Our loglinear model has an AUC value of 0.77 (Fig. 7a). The
inhomogeneous K-function shown in Fig. 7b quantifies the expected number of points as a function of distance from each
point, adjusted for the modeled inhomogeneous intensity of the point pattern. Distances between individual landslides are
calculated as the shortest-path distance along the road rather than the direct Euclidean distance. Acceptance intervals around
the theoretical K-function were derived from repeated simulations of the inhomogeneous Bayesian loglinear model. The
actual point pattern's K-function is outside these acceptance intervals, suggesting a clustering that cannot be explained by the
covariates. A comparison of 100 randomly simulated and actual point densities (Fig. 7c) shows that the modeled and
observed spatial landslide densities are consistent although the second, smaller peak of landslide densities close to Joshimath
are not well captured by the model. Moreover, 5-fold cross-validation based on 15-km long road segments reveals AUC-
values between 0.75 and 0.76.

Can the model be improved by incorporating more explanatory covariates? Our impression in the field was that landslides
detach independently of planform hillslope geometry as they occurred both on spurs and convex hollows. Nevertheless, we
calculated total curvature and topographic roughness as potential predictor candidates. In addition, we used landcover (Table
3) and distance to faults (Fig. 1) as they are commonly used in susceptibility studies (e.g., Stanley and Kirschbaum 2017, Li
et al., 2020, Ozturk et al., 2021) and potentially control the density of road-side slope failures. Yet, including these metrics in
the model barely contributes to improving the model fit and their incorporation in the model would, according to the AIC,
lead to overfitting (Fig. 8).

5 Discussion

We recorded more than one landslide per road kilometer along the NH-7 between Rishikesh and Joshimath. The fact that this
road is strongly affected by landslides has been previously described and attributed to the region's fragility of slopes,
focused rainfall and frequent seismicity (Sati et al., 2011). In addition to the environmental conditions, road construction and
widening have contributed to the formation of new landslides, which are often shallow and small, but nevertheless lead to
fatalities, inflict severe damages to infrastructure and cause traffic disruption (Sati et al., 2011). We conducted a systematic
survey of road-side landslides and derived a statistical model that aims at quantifying landslide exposure along the NH-7 at a
high spatial resolution.

Our analysis relied on a GPS-based survey of landslides while traveling from Rishikesh to Joshimath shortly after a period of
anomalously high rainfall. Using this approach, we mapped landslides irrespective of cloud cover and without acquiring
high-resolution satellite imagery, which is needed to detect small landslides. A drawback, however, is that we may have
missed landslides where debris had already been removed by road works. Also, detailed mapping of the areal extent of the

280   landslides was not possible during drive-by so that we did not quantify the size of landslides. Thus, our modeling approach treats all landslides the same, irrespective of their areal extent and volume. To this end, however, this enables us to adopt a modeling approach, which conceptualizes landslides as an unmarked network-attached point pattern (Baddeley et al., 2021; Okabe and Sugihara, 2012). Representing landslides as network-attached points and not as areal features entails advantages and disadvantages. Constraining landslide locations to lie on roads demands that all predictor variables also need to be

285   mapped to the road network, which entails some generalization and additional degrees of freedom about the choice and aggregation of 2D variables. For landslide susceptibility analysis, for example, this means that spatial variables characterizing the source area (e.g., hillslope gradient) are projected onto the road. At the same time, model development and fitting benefits from smaller sample sizes as data amounts are moderate and computational demands during Bayesian posterior sampling remain manageable.

290

We detected a profound difference between rainfall products, for which a detailed analysis is outside the scope of this study. These differences have been recognized before by several studies along the Himalayan orographic front and have either been attributed to the network of rain gauges, which is particularly sparse at high elevations, or, if rainfall estimates are based on remote sensing data, to irregular return times, owing to which individual rainfall events may be missed (Andermann et al.,

295   2011, Hu et al., 2016). To this end, these uncertainties are crucial for capturing the spatial patterns of landslides (Ozturk et al., 2021). We found that CHIRPS v2 performed best in predicting the spatial landslide patterns along NH-7 but the employed search strategy must be viewed critically as the reverse conclusion, that landslides are controlled by these patterns is not necessarily true. Indeed, studies come to different conclusions about the performance of CHIRPS v2 and other gridded rainfall products (Kumar et al., 2021). Based on the analysis of 18 extreme precipitation events during 2014–16 in the

300   northwest Himalaya (including our study site), however, Jena et al. (2020) conclude that CHIRPS v2 provides the most reliable precipitation estimates. Moreover, the two-peaked rainfall pattern of CHIRPS v2 is most consistent with long-term rainfall patterns obtained from the interpolation of 44 rainfall gauge records averaging over the period from 1901 to 1950, which show highest values along the Himalayan Front and the physiographic transition to the High Himalaya (Basistha et al., 2008; Bookhagen, 2010).

305

Lithozones derived from a geological map contributed to the explanatory power of the model, thus highlighting the role of lithological properties in modulating landslide susceptibility. As we did not measure the actual geotechnical and -mechanical properties or e.g., bedding and foliation along our route, we can only provide a first order reasoning of the prediction capacity of the lithozones. The high landslide density in lithozone 2 is likely related to the pronounced fissility and cleavage

310   of the dominating shales and phyllites. Moreover, material softening, percolation and weathering cause a general decrease in rock strength. Tectonic activity adds to a general decrease in rock strength by creating shear surfaces with low friction angles (Stead, 2016). In addition, road segments, where the adjoining hillslopes parallel bedding, joints or foliation planes are particularly vulnerable (e.g., Bartarya and Valdiya, 1989). Conversely, lithozone 4 is characterized by quartzite and igneous rocks. These have undergone low- to high-grade metamorphism and are generally harder and have a more irregular fabric

315   that restrains the formation of planar slide surfaces. Moreover, these rocks tend to develop more stable regolith mantles (Gerrard, 1994), and are thus less susceptible to landsliding. Our model shows that under the same topographic conditions and rainfall amounts, the rock types of lithozone 2 are 2–6 times more susceptible to landslides than those in lithozone 4 (Fig. 6c). The remaining lithozones are not credibly different from each other. In part, the lack of differences can be attributed to the low number of samples as only a small fraction of the road traverses these lithozones (Table 2).

320   Notwithstanding, a general trend towards lower landslide susceptibility from lithozone 1–5 are consistent with a previous review study about lithological controls on the occurrence of mass movements in the Himalaya (Gerrard, 1994).

Previous studies indicate that human activities have played a crucial role in predisposing slopes to failure (Li et al., 2020; van Westen et al., 2008; Tanyas et al., 2022). Our analysis underscores these findings and quantifies the occurrence of
325   landslides to be twice as high along widened sections of NH-7, if corrected for the influence of the other predictor variables. The process of cutting into mountain sides to create wider pathways often creates unstable slopes that are prone to failure (Barnard et al., 2001; Haigh & Rawat, 2011; Sati et al., 2011; Li et al., 2020). The removal of trees and vegetation for road widening removes their stabilizing effect on slopes, further increasing the likelihood of landslides (e.g., Guthrie, 2002). Additionally, widened roads can lead to increased surface runoff during heavy rainfall or snowmelt, saturating the soil and
330   making it more susceptible to landslides (e.g., Wadhawan et al., 2020). Rock blasting required during the road widening process can lead to the fracturing and weakening of rock masses, creating potential landslide-prone zones along the road corridors (Sati et al., 2011). Moreover, the alteration of natural drainage patterns due to road widening can redirect water flow and potentially cause erosion and instability on adjacent slopes. In fact, these disturbances have led to frequent landslides along the NH-7 previously as Sati et al. (2011) also report about ~300 landslides occurring along the road more
335   than 10 years ago. Our data indicates that 20–40 % of the recorded landslides are reactivated slope failures which highlights that slopes are recurrently unstable during periods with intense rainfall (Joshi and Kumar, 2006). During mapping, we also noticed that some slopes were engineered during the last years with retaining walls, yet many of which also failed.

Our model may miss important predictor variables that control the occurrence of landslides. We included variables that
340   characterize environmental conditions and found that slope, rainfall, road widening and lithology largely explain the variability in landslide density. Variables such as landuse or topographic derivatives do not improve the performance of the model as measured by the AIC, at least at the spatial scale at which these variables were available. However, we cannot exclude that small-scale topographic changes due to construction or land use changes (e.g. abandonment and degradation of agricultural fields and terrace systems) may exacerbate road-side slope failures (Jacquet et al., 2015; Mauri et al., 2022).

345

Our model hindcasts the spatial pattern of road-blocking landslides and we posit that it can be used as a time-predictive model as well. Rainfall is one of the main covariates in the model and is also the one with the largest uncertainties as shown by the discrepancies of gridded rainfall products. A denser network of rain gauges and a better availability of this data would likely contribute, together with weather forecasting, to more accurate estimates of landslide occurrences, which ultimately
350   would facilitate a more efficient allocation of resources for road maintenance. Also, recurrent slope failures should be monitored more closely to direct efforts for slope reinforcements. The land cover data, which we included in the model, is too coarse to capture the widespread lack of vegetation along the road. As many of the landslides were shallow, revegetating slopes may contribute to their stabilization.

355   To this end, the NH-7 is a key arterial road and landslides make transport of goods and people difficult, thus causing serious economic disruption. Moreover, slope failures along the road have led to fatalities in parts where roads were widened, and recent heavy rainfalls in July 2023 have caused several severe landslides[2]. Such damages and commensurate fatalities may become even more frequent in the future. The entire Upper Ganga basin is susceptible to extreme rainfall events (Joshi and Kumar, 2006), and climate change projections – although subject to high uncertainties – indicate a trend towards more
360   frequent extreme events due to elevation-dependent warming and a likely increase of summer monsoon precipitation by 4– 25 % (Krishnan et al., 2019). In addition, exposure to landslides is likely to increase in Uttarakhand as the Char Dham National Highway project gets implemented (Chouhan et al., 2022). Road construction and increased traffic volumes attract more people, who will strive for new economic opportunities associated with sites along roads (Fort et al., 2010; Chouhan et

---

[2]https://www.hindustantimes.com/india-news/landslide-on-char-dham-road-leaves-pilgrims-stranded-heavy-rains-cause-damage-and-blockages-in-uttarakhand-101690225215947.html

al., 2022). These sites are often more susceptible to landslides as construction often implies vegetation removal and slope
365 destabilization (Petley et al., 2007, Li et al., 2020). A reduction of traffic may disrupt the cycle of increasing hazard and
exposure. The commissioning of the currently constructed 125 km long broad-gauge railway between Rishikesh and
Karnprayag (Azad et al., 2022) might be a major step towards this goal.

6 Conclusions

Road construction is soaring in the Himalayas. During the last five years, ~11,000 km of roads were built in the Indian
370 Himalayan states (The Tribune, 2022). Yet, the fragility of the Himalayan landscape as well as slope undercutting and poor
construction practices make maintenance of these roads challenging. Our study of landslides along the NH-7 demonstrates
the scale of this challenge as we detect more than one partially or fully road-blocking landslide per road kilometer between
Rishikesh and Joshimath. We contribute to a better understanding and prediction of these landslides by creating a landslide
inventory of road-side landslides and the adoption of a novel approach to landslide exposure analysis, which treats the
375 landslides as unmarked network-attached spatial point phenomena. Together with inhomogeneous Poisson process models,
this inventory enables us to identify the main controlling variables, i.e., slope angle, rainfall amount, road widening and
lithology. Our model shows that, if corrected for all other influences, road widening leads to a doubling of road-blocking
landslides. This finding quantitatively underpins previous claims that improper construction practices of road widening
increase, rather than decrease landslide hazards along roads (Sati et al., 2011). The Himalaya's fragile geology and exposure
380 to torrential rains demand proper geological assessments and mitigation measures, such as constructing retaining walls,
installing drainage systems, and stabilizing slopes, to minimize the impact of road widening on landslide occurrence.
Thorough environmental impact assessments before road widening projects and consideration of alternative routes or
transportation solutions can help strike a balance between development and preserving the delicate mountain ecosystem
while reducing landslide risks.

385

Code and data availability. The code and data to run the analysis are available in the supplemental data.

Author contributions. All authors conceived the study and conducted mapping landslides. RKG retrieved and analyzed the
rainfall data. JM and AP compiled, analyzed and visualized the data and WS conducted the statistical analysis. All authors
390 wrote the manuscript.

Acknowledgments. We acknowledge the German Exchange Service (DAAD) for funding the project Co-PREPARE (Project-
ID: 57553291), a joint project of the IIT Roorkee and University of Potsdam. JM acknowledges financial support from the
Research Focus "Earth and Environmental Systems" of the University of Potsdam. RKG acknowledges the financial support
395 received from the Prime Minister's Research Fellowship, Government of India for Grant number PM-31-22-695-414.

References

Adhikari, D., Tiwary, R., Singh, P. P., Suchiang, B. R., Nonghuloo, I. M., and Barik, S. K.: Trees, Shrubs and Herbs for
Slope Stabilization in Landslide Prone Areas of Eastern Himalaya BT - Nature-based Solutions for Resilient
Ecosystems and Societies, edited by: Dhyani, S., Gupta, A. K., and Karki, M., Springer Singapore, Singapore, 307–326,
400 https://doi.org/10.1007/978-981-15-4712-6_18, 2020.
Akaike, H.: A new look at the statistical model identification. IEEE transactions on automatic control, 19(6), 716-723, 1974.
Andermann, C., Bonnet, S., and Gloaguen, R.: Evaluation of precipitation data sets along the Himalayan front,
Geochemistry, Geophys. Geosystems, 12, https://doi.org/10.1029/2011GC003513, 2011.

405   Ang, Q., Baddeley, A., and Nair, G.: Geometrically Corrected Second Order Analysis of Events on a Linear Network, with
         Applications to Ecology and Criminology, Scand. J. Stat., 39, 591–617, https://doi.org/10.1111/j.1467-
         9469.2011.00752.x, 2012.

Asthana, B. N. and Khare, D.: Hill Slope Stabilization at Dam and Power Projects in Himalayas BT - Recent Advances in
         Dam Engineering, edited by: Asthana, B. N. and Khare, D., Springer International Publishing, Cham, 239–264,
         https://doi.org/10.1007/978-3-030-32278-6_11, 2022.

410   Azad, M. A., Singh, S. K., Alok, A., Meenakshi, Shekhar, S., and Kumar, P.: Geotechnical and geological studies of Adit-6
         of the railway tunnel between Rishikesh and Karnprayag in India focusing on the excavation methods and design of
         support analysis: a case study, Arab. J. Geosci., 15, 129, https://doi.org/10.1007/s12517-021-09355-7, 2022.

Baddeley, A., Nair, G., Rakshit, S., McSwiggan, G., and Davies, T. M.: Analysing point patterns on networks — A review,
         Spat. Stat., 42, 100435, https://doi.org/10.1016/J.SPASTA.2020.100435, 2021.

415   Baddeley, A., Rubak, E., and Turner, R.: Spatial point patterns: methodology and applications with R, CRC press, 2015.

Barnard, P. L., Owen, L. A., Sharma, M. C., and Finkel, R. C.: Natural and human-induced landsliding in the Garhwal
         Himalaya of northern India, Geomorphology, 40, 21–35, https://doi.org/10.1016/S0169-555X(01)00035-6, 2001.

Bartarya, S. K. and Valdiya, K. S.: Landslides and Erosion in the Catchment of the Gaula River, Kumaun Lesser Himalaya,
         India, Mt. Res. Dev., 9, 405, 1989.

420   Basistha, A., Arya, D. S., and Goel, N. K.: Spatial Distribution of Rainfall in Indian Himalayas – A Case Study of
         Uttarakhand Region, Water Resour. Manag., 22, 1325–1346, https://doi.org/10.1007/s11269-007-9228-2, 2008.

Beck, H. E., Vergopolan, N., Pan, M., Levizzani, V., van Dijk, A. I. J. M., Weedon, G. P., Brocca, L., Pappenberger, F.,
         Huffman, G. J., and Wood, E. F.: Global-scale evaluation of 22 precipitation datasets using gauge observations and
         hydrological modeling, Hydrol. Earth Syst. Sci., 21, 6201–6217, https://doi.org/10.5194/hess-21-6201-2017, 2017.

425   Bollinger, L., Sapkota, S. N., Tapponnier, P., Klinger, Y., Rizza, M., Van der Woerd, J., Tiwari, D. R., Pandey, R., Bitri, A.,
         and Bes de Berc, S.: Estimating the return times of great Himalayan earthquakes in eastern Nepal: Evidence from the
         Patu and Bardibas strands of the Main Frontal Thrust, J. Geophys. Res. Solid Earth, 119, 7123–7163,
         https://doi.org/10.1002/2014JB010970, 2014.

Bookhagen, B.: Appearance of extreme monsoonal rainfall events and their impact on erosion in the Himalaya, Geomatics,
430   Nat. Hazards Risk, 1, 37–50, https://doi.org/10.1080/19475701003625737, 2010.

Buchhorn, M., Smets, B., Bertels, L., Roo, B. De, Lesiv, M., Tsendbazar, N.-E., Li, L., and Tarko, A.: Copernicus Global
         Land Service: Land Cover 100m: version 3 Globe 2015-2019: Product User Manual,
         https://doi.org/10.5281/zenodo.3938963, 2020.

Chouhan, S., Thieken, A. H., Bubeck, P., and Mukherjee, M.: Role of tourism on disaster recovery: A case study of
435   Uttarakhand, India, Int. J. Disaster Risk Reduct., 95, 103878, https://doi.org/https://doi.org/10.1016/j.ijdrr.2023.103878,
         2023.

Das, I., Stein, A., Kerle, N., and Dadhwal, V. K.: Landslide susceptibility mapping along road corridors in the Indian
         Himalayas using Bayesian logistic regression models, Geomorphology, 179, 116–125,
         https://doi.org/10.1016/j.geomorph.2012.08.004, 2012.

440   Devkota, K. C., Regmi, A. D., Pourghasemi, H. R., Yoshida, K., Pradhan, B., Ryu, I. C., Dhital, M. R., and Althuwaynee, O.
         F.: Landslide susceptibility mapping using certainty factor, index of entropy and logistic regression models in GIS and
         their comparison at Mugling–Narayanghat road section in Nepal Himalaya, Nat. Hazards, 65, 135–165,
         https://doi.org/10.1007/s11069-012-0347-6, 2013.

European Space Agency, Sinergise. Copernicus Global Digital Elevation Model. Distributed by OpenTopography, Accessed:
445   2022-12-27, https://doi.org/10.5069/G9028PQB, 2021.

Evans, I. S.: Geomorphometry and landform mapping: What is a landform?, Geomorphology, 137, 94–106, https://doi.org/10.1016/j.geomorph.2010.09.029, 2012.

Fort, M., Cossart, E., and Arnaud-Fassetta, G.: Hillslope-channel coupling in the Nepal Himalayas and threat to man-made structures: The middle Kali Gandaki valley, Geomorphology, 124, 178–199,

450   https://doi.org/https://doi.org/10.1016/j.geomorph.2010.09.010, 2010.

Funk, C., Peterson, P., Landsfeld, M., Pedreros, D., Verdin, J., Shukla, S., Husak, G., Rowland, J., Harrison, L., Hoell, A., and Michaelsen, J.: The climate hazards infrared precipitation with stations—a new environmental record for monitoring extremes, Sci. Data, 2, 150066, https://doi.org/10.1038/sdata.2015.66, 2015.

Geological Survey of India: Uttarakhand lithology, Government of India, Kolkata, India, 08.10.2022,

455   https://bhukosh.gsi.gov.in, 2022.

Gerrard, J.: The landslide hazard in the Himalayas: geological control and human action, edited by: Morisawa, M. B. T.-G. and N. H., Elsevier, Amsterdam, 221–230, https://doi.org/10.1016/B978-0-444-82012-9.50019-0, 1994.

Guthrie, R. H.: The effects of logging on frequency and distribution of landslides in three watersheds on Vancouver Island, British Columbia, *Geomorphology*, *43*(3-4), 273-292, 2002.

460   Haigh, M. J.: Landslide prediction and highway maintenance in the Lesser Himalaya, India, Zeitschrift für Geomorphol. Suppl., 51, 17–38, 1984.

Haigh, M. and Rawat, J. S.: Landslide causes : Human impacts on a Himalayan landslide swarm, Belgian J. Geogr., 3–4, 201–220, https://doi.org/10.4000/belgeo.6311, 2011.

Hanley, J. A. and McNeil, B. J.: The meaning and use of the area under a receiver operating characteristic (ROC) curve,

465   Radiology, 143(1), 29-36, 1982.

Hu, Z., Hu, Q., Zhang, C., Chen, X., and Li, Q.: Evaluation of reanalysis, spatially interpolated and satellite remotely sensed precipitation data sets in central Asia, J. Geophys. Res. Atmos., 121, 5648–5663, https://doi.org/10.1002/2016JD024781, 2016.

Huffman, G.J., E.F. Stocker, D.T. Bolvin, E.J. Nelkin, Jackson Tan, GPM IMERG Late Precipitation L3 1 day 0.1 degree x

470   0.1 degree V06, Edited by Andrey Savtchenko, Greenbelt, MD, Goddard Earth Sciences Data and Information Services Center (GES DISC), Accessed: July 3, 2023, https://doi.org/10.5067/GPM/IMERGDL/DAY/06, 2019

Jaquet, S., Schwilch, G., Hartung-Hofmann, F., Adhikari, A., Sudmeier-Rieux, K., Shrestha, G., Liniger, H. P., and Kohler, T.: Does outmigration lead to land degradation? Labour shortage and land management in a western Nepal watershed, Appl. Geogr., 62, 157–170, https://doi.org/https://doi.org/10.1016/j.apgeog.2015.04.013, 2015.

475   Jena, P., Garg, S., and Azad, S.: Performance Analysis of IMD High-Resolution Gridded Rainfall (0.25° × 0.25°) and Satellite Estimates for Detecting Cloudburst Events over the Northwest Himalayas, J. Hydrometeorol., 21, 1549–1569, https://doi.org/10.1175/JHM-D-19-0287.1, 2020.

Joshi, V. and Kumar, K.: Extreme rainfall events and associated natural hazards in Alaknanda valley, Indian Himalayan region, J. Mt. Sci., 3, 228–236, https://doi.org/10.1007/s11629-006-0228-0, 2006.

480   Kanungo, D. P., Pain, A., and Sharma, S.: Finite element modeling approach to assess the stability of debris and rock slopes: a case study from the Indian Himalayas, Nat. Hazards, 69, 1–24, https://doi.org/10.1007/s11069-013-0680-4, 2013.

Kayal, J. R., Ram, S., Singh, O. P., Chakraborty, P. K., and Karunakar, G.: Aftershocks of the March 1999 Chamoli Earthquake and Seismotectonic Structure of the Garhwal Himalaya, Bull. Seismol. Soc. Am., 93, 109–117, 2003.

Koushik, P., Shantanu, S., Manojit, S., and Mahesh, S.: Stability analysis and design of slope reinforcement techniques for a

485   Himalayan landslide BT - Proceedings of the conference on Recent Advances in Rock Engineering (RARE 2016), 97– 104, https://doi.org/10.2991/rare-16.2016.16, 2016.

Krishnan, R., Shrestha, A. B., Ren, G., Rajbhandari, R., Saeed, S., Sanjay, J., Syed, M. A., Vellore, R., Xu, Y., You, Q., and Ren, Y.: Unravelling Climate Change in the Hindu Kush Himalaya: Rapid Warming in the Mountains and Increasing

Extremes - The Hindu Kush Himalaya Assessment: Mountains, Climate Change, Sustainability and People, edited by:
490   Wester, P., Mishra, A., Mukherji, A., and Shrestha, A. B., Springer International Publishing, Cham, 57–97,
       https://doi.org/10.1007/978-3-319-92288-1_3, 2019.

Kumar, M., Hodnebrog, Ø., Sophie Daloz, A., Sen, S., Badiger, S., and Krishnaswamy, J.: Measuring precipitation in
       Eastern Himalaya: Ground validation of eleven satellite, model and gauge interpolated gridded products, J. Hydrol., 599,
       126252, https://doi.org/10.1016/j.jhydrol.2021.126252, 2021.

495   Kundu, J., Sarkar, K., and Singh, A. K.: Integrating structural and numerical solutions for road cut slope stability analysis-a
       case study, India, in: ISRM 2nd International Conference on Rock Dynamics, 2016.

Lave, J. and Avouac, J. P.: Fluvial incision and tectonic uplift across the Himalayas of central Nepal, J. Geophys. Res., 106,
       2001.

Li, Y., Wang, X., and Mao, H.: Influence of human activity on landslide susceptibility development in the Three Gorges
500   area, Nat. Hazards, 104, 2115–2151, https://doi.org/10.1007/s11069-020-04264-6, 2020.

Lombardo, L., Bakka, H., Tanyas, H., van Westen, C., Mai, P. M., and Huser, R.: Geostatistical Modeling to Capture
       Seismic-Shaking Patterns From Earthquake-Induced Landslides, J. Geophys. Res. Earth Surf., 124, 1958–1980,
       https://doi.org/10.1029/2019JF005056, 2019.

Lombardo, L., Opitz, T., and Huser, R.: Point process-based modeling of multiple debris flow landslides using INLA: an
505   application to the 2009 Messina disaster, Stoch. Environ. Res. Risk Assess., 32, 2179–2198,
       https://doi.org/10.1007/s00477-018-1518-0, 2018.

Makalic, E. and Schmidt, D. F.: A Simple Bayesian Algorithm for Feature Ranking in High Dimensional Regression
       Problems. AI 2011: Advances in Artificial Intelligence, 223–230, 2011.

Makalic, E. and Schmidt, D. F.: High-Dimensional Bayesian Regularised Regression with the BayesReg Package, arXiv.
510   https://doi.org/10.48550/ARXIV.1611.06649, 2016.

Mauri, L., Straffelini, E., and Tarolli, P.: Multi-temporal modeling of road-induced overland flow alterations in a terraced
       landscape characterized by shallow landslides, Int. Soil Water Conserv. Res., 10, 240–253,
       https://doi.org/https://doi.org/10.1016/j.iswcr.2021.07.004, 2022.

Meyer, N. K., Schwanghart, W., Korup, O., and Nadim, F.: Roads at risk: traffic detours from debris flows in southern
515   Norway, Nat. Hazards Earth Syst. Sci., 15, 985–995, https://doi.org/10.5194/nhess-15-985-2015, 2015.

Mitra, A. K., Bohra, A. K., Rajeevan, M. N., and Krishnamurti, T. N.: Daily Indian Precipitation Analysis Formed from a
       Merge of Rain-Gauge Data with the TRMM TMPA Satellite-Derived Rainfall Estimates, J. Meteorol. Soc. Japan. Ser.
       II, 87A, 265–279, https://doi.org/10.2151/jmsj.87A.265, 2009.

National Crime Records Bureau: Accidental Deaths & Suicides in India 2021, https://ncrb.gov.in/en/node/3722, 2022.

520   Okabe, A., Okunuki, K., and Shiode, S.: SANET: A Toolbox for Spatial Analysis on a Network, Geogr. Anal., 38, 57–66,
       https://doi.org/10.1111/j.0016-7363.2005.00674.x, 2006.

Okabe, A. and Sugihara, K.: Spatial analysis along networks: statistical and computational methods, John Wiley & Sons,
       2012.

Ozturk, U., Saito, H., Matsushi, Y., Crisologo, I., and Schwanghart, W.: Can global rainfall estimates (satellite and
525   reanalysis) aid landslide hindcasting?, Landslides, 18, 3119–3133, https://doi.org/10.1007/s10346-021-01689-3, 2021.

Pai, D. S., Sridhar, L., Rajeevan, M., Sreejith, O. P., Satbhai, N. S., and Mukhopadhyay, B.: Development of a new high
       spatial resolution ($0.25° \times 0.25°$) long period (1901-2010) daily gridded rainfall data set over India and its comparison
       with existing data sets over the region, MAUSAM, 1, 1–18, https://doi.org/10.54302/mausam.v65i1.851, 2014.

Petley, D. N., Hearn, G. J., Hart, A., Rosser, N. J., Dunning, S. A., Oven, K., and Mitchell, W. A.: Trends in landslide
530   occurrence in Nepal, Nat. Hazards, 43, 23–44, https://doi.org/10.1007/s11069-006-9100-3, 2007.

Prasad, S. and Siddique, T.: Stability assessment of landslide-prone road cut rock slopes in Himalayan terrain: A finite element method based approach, J. Rock Mech. Geotech. Eng., 12, 59–73, https://doi.org/10.1016/j.jrmge.2018.12.018, 2020.

535 Rajendran, K., Parameswaran, R. M., and Rajendran, C. P.: Seismotectonic perspectives on the Himalayan arc and contiguous areas: Inferences from past and recent earthquakes, Earth-Science Rev., 173, 1–30, https://doi.org/10.1016/j.earscirev.2017.08.003, 2017.

Rawat, M. S., Joshi, V., Uniyal, D. P., and Rawat, B. S.: Investigation of hill slope stability and mitigation measures in Sikkim Himalaya, Int. J. Landslide Environ., 3, 8–15, 2016.

Sarkar, S. and Kanungo, D. P.: Landslides in the Alaknanda Valley of Garhwal Himalaya, India, Q. J. Eng. Geol.
540 Hydrogeol., 39, 79–82, https://doi.org/10.1144/1470-9236/05-020, 2006.

Sati, S. P., Sundriyal, Y., Rana, N., and Dangwal, S.: Recent landslides in Uttarakhand: nature's fury or human folly, Curr. Sci., 100, 2011.

Schwanghart, W. and Scherler, D.: Bumps in river profiles: uncertainty assessment and smoothing using quantile regression techniques, Earth Surf. Dyn., 5, 821–839, https://doi.org/10.5194/esurf-5-821-2017, 2017.

545 Schwanghart, W. and Scherler, D.: Short Communication: TopoToolbox 2 – MATLAB-based software for topographic analysis and modeling in Earth surface sciences, Earth Surf. Dyn., 2, 1–7, https://doi.org/10.5194/esurf-2-1-2014, 2014.

Schwanghart, W., Molkenthin, C., and Scherler, D.: A systematic approach and software for the analysis of point patterns on river networks, Earth Surf. Process. Landforms, 46, 1847–1862, https://doi.org/10.1002/esp.5127, 2021.

Shugar, D. H., Jacquemart, M., Shean, D., Bhushan, S., Upadhyay, K., Sattar, A., Schwanghart, W., McBride, S., van Wyk
550 de Vries, M., Mergili, M., Emmer, A., Deschamps-Berger, C., McDonnell, M., Bhambri, R., Allen, S., Berthier, E., Carrivick, J. L., Clague, J. J., Dokukin, M., Dunning, S. A., Frey, H., Gascoin, S., Haritashya, U. K., Huggel, C., Kääb, A., Kargel, J. S., Kavanaugh, J. L., Lacroix, P., Petley, D., Rupper, S., Azam, M. F., Cook, S. J., Dimri, A. P., Eriksson, M., Farinotti, D., Fiddes, J., Gnyawali, K. R., Harrison, S., Jha, M., Koppes, M., Kumar, A., Leinss, S., Majeed, U., Mal, S., Muhuri, A., Noetzli, J., Paul, F., Rashid, I., Sain, K., Steiner, J., Ugalde, F., Watson, C. S., and Westoby, M. J.: A
555 massive rock and ice avalanche caused the 2021 disaster at Chamoli, Indian Himalaya, Science, 373, 300–306, https://doi.org/10.1126/science.abh4455, 2021.

Siddique, T. and Pradhan, S. P.: Stability and sensitivity analysis of Himalayan road cut debris slopes: an investigation along NH-58, India, Nat. Hazards, 93, 577–600, https://doi.org/10.1007/s11069-018-3317-9, 2018.

Siddique, T., Pradhan, S. P., Vishal, V., Mondal, M. E. A., and Singh, T. N.: Stability assessment of Himalayan road cut
560 slopes along National Highway 58, India, Environ. Earth Sci., 76, 1–18, 2017.

Singh, R., Umrao, R. K., and Singh, T. N.: Stability evaluation of road-cut slopes in the Lesser Himalaya of Uttarakhand, India: conventional and numerical approaches, Bull. Eng. Geol. Environ., 73, 845–857, 2014.

Stanley, T. and Kirschbaum, D. B.: A heuristic approach to global landslide susceptibility mapping, Nat. Hazards, 87, 145–164, https://doi.org/10.1007/s11069-017-2757-y, 2017.

565 Stead, D.: The Influence of Shales on Slope Instability, Rock Mech. Rock Eng., 49, 635–651, https://doi.org/10.1007/s00603-015-0865-0, 2016.

Sur, U., Singh, P., and Meena, S. R.: Landslide susceptibility assessment in a lesser Himalayan road corridor (India) applying fuzzy AHP technique and earth-observation data, Geomatics, Nat. Hazards Risk, 11, 2176–2209, https://doi.org/10.1080/19475705.2020.1836038, 2020.

570 Swarnkar, S., Mujumdar, P., and Sinha, R.: Modified hydrologic regime of upper Ganga basin induced by natural and anthropogenic stressors, Sci. Rep., 1–11, https://doi.org/10.1038/s41598-021-98827-7, 2021.

Tanyaş, H., Görüm, T., Kirschbaum, D., and Lombardo, L.: Could road constructions be more hazardous than an earthquake in terms of mass movement?, Nat. Hazards, 112, 639–663, https://doi.org/10.1007/s11069-021-05199-2, 2022.

The Tribune, India: https://www.tribuneindia.com/news/nation/10-969-km-roads-in-himalayan-states-461738, last access: 29
575   December 2022.

United States Geological Survey (USGS), Earthquake Catalog, https://earthquake.usgs.gov/earthquakes/search/, last access:
         27 November 2022.

Uniyal, A.: Infra Development Vision for Himalaya in the Aftermath of Rishiganga Tragedy, Disaster & Development, 149–
         159 pp., 2021.

580   van Westen, C. J., Castellanos, E., and Kuriakose, S. L.: Spatial data for landslide susceptibility, hazard, and vulnerability
         assessment: An overview, Eng. Geol., 102, 112–131, https://doi.org/10.1016/j.enggeo.2008.03.010, 2008.

Wadhawan, S. K., Singh, B., & Ramesh, M. V.: Causative factors of landslides 2019: case study in Malappuram and
         Wayanad districts of Kerala, India, *Landslides*, *17*, 2689-2697, 2020.

Wang, Q., Zhang, P.-Z., Freymueller, J. T., Bilham, R., Larson, K. M., Lai, X., You, X., Niu, Z., Wu, J., Li, Y., Liu, J.,
585   Yang, Z., and Chen, Q.: Present-Day Crustal Deformation in China Constrained by Global Positioning System
         Measurements, Science, 294, 574–577, https://doi.org/10.1126/science.1063647, 2001.
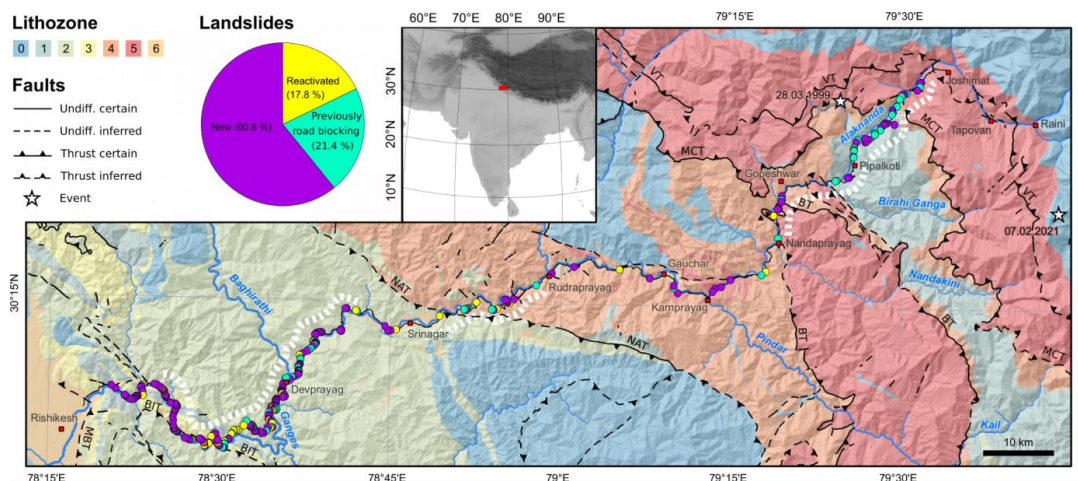
Figures

Figure 1: Map of the study site. Landslides, lithozones and major faults along NH-7 from Rishikesh to Joshimath. The
590   highest density of landslides occurs between Rishikesh and Srinagar within lithozone 2 and between Pipalkoti and Joshimath
in lithozone 1. For description of the lithozones see Table 2. Note that lithozones 0 and 6 are not crossed by the road and are
therefore omitted from the description. We subdivided the landslides into new ones, reactivated ones and those that were
blocking the road before September 2022. White stippled lines indicate the road segments that have undergone widening
(Sati et al., 2011). Lithozones and faults were modified from digital maps provided by the Geological Survey of India
595   (2022). Stars indicate locations of the 1999 M_w 6.6 Chamoli earthquake (Kayal et al., 2003; USGS, 2022) and the 2021
Chamoli rock and ice avalanche (Shugar et al., 2021). MBT: Main Boundary Thrust, BIT: Bijni Thrust, NAT: North Almora
Thrust, BT: Baijnat Thrust, MCT: Main Central Thrust, VT: Vaikrita Thrust.

Figure 2: Examples of partially road-blocking landslides along the highway NH-7. Panels a) and c) show locations, where hillslopes parallel the foliation/bedding.

600
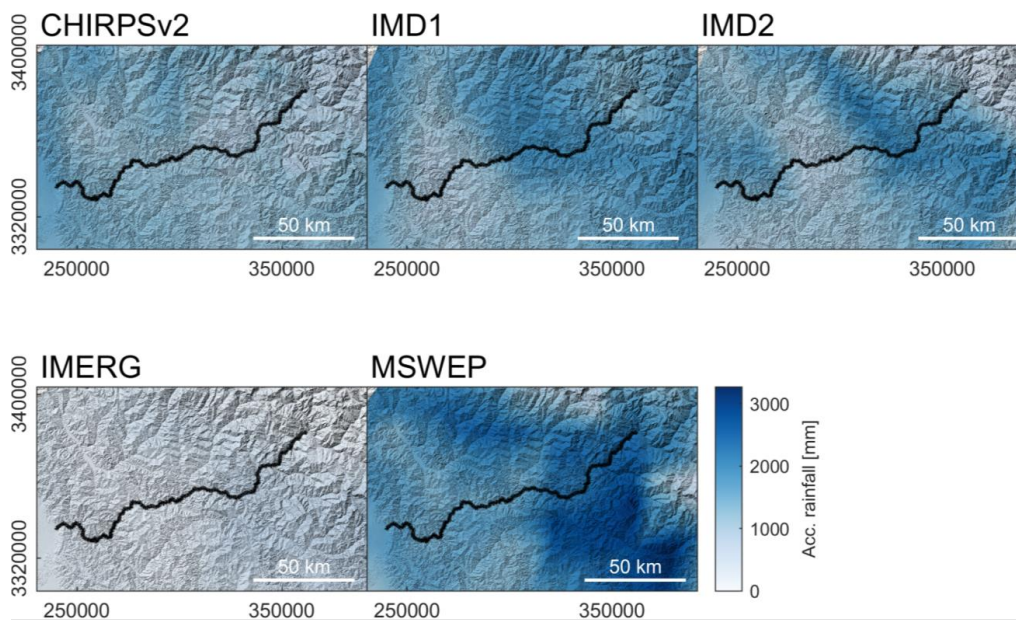
Figure 3: Accumulated rainfall amounts from different rainfall products between Jan 1 and Oct 10, 2023. The black line indicates the road between Rishikesh and Joshimath (see Fig. 1).
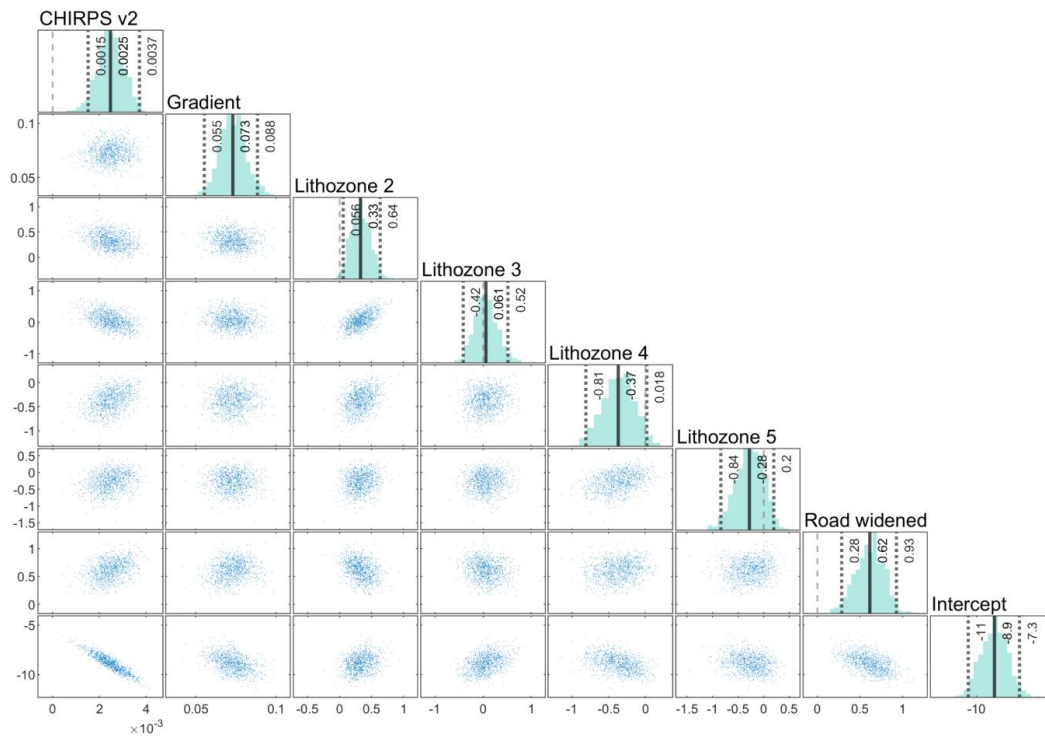
605

Figure 4: Posterior parameter samples of the loglinear model of landslide occurrence along the NH-7. CHIRPS v2 is the gridded rainfall product, gradient determines the slope within 210 m to the road and lithozones were aggregated from a geological map. Note that Lithozone 1 is missing since the parameter is encapsulated in the intercept.
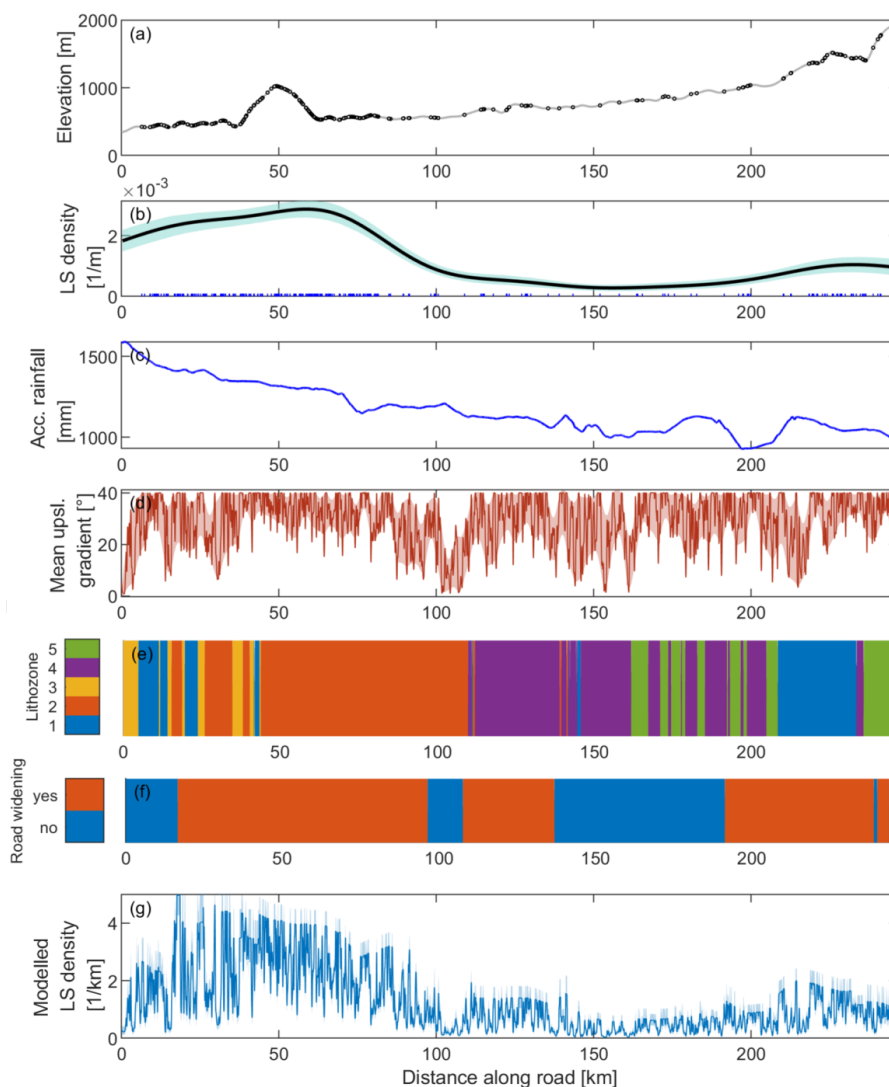
Figure 5: Predictor and response variables used in the model. a) shows the occurrences of the fully and partially road-blocking landslides together with the elevation profile of the road. b) Landslide density along the road using a Gaussian kernel and 15 km bandwidth as well as bootstrapped confidence bounds. c) Accumulated rainfall between January 1 to October 10, 2022 from CHIRPS v2. d) Mean upslope gradient within a distance of 210 m around the road. The shaded area denotes the 5 and 95 **%** bounds using a nonparametric quantile regression and highlights the larger scale variability of the gradient. e) Lithozones along the road (see also Fig. 1). f) Widened road segments. g) Predicted landslide density using a model involving rainfall, slope and lithozones as covariates.
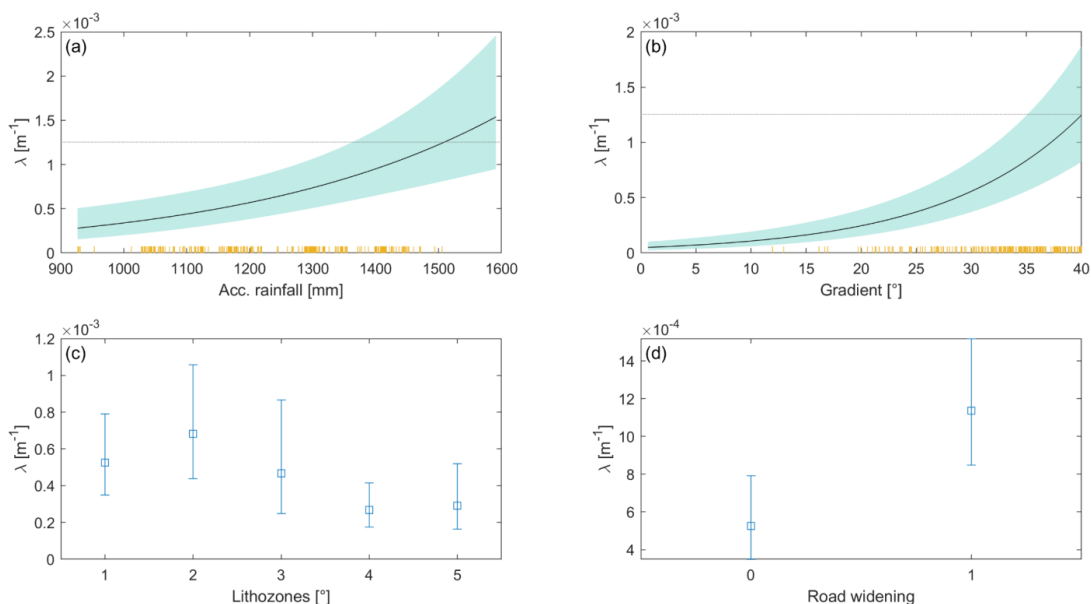
Figure 6: Main effects of predictors in the loglinear model of road-blocking landslides along the NH-7. a) Effect of accumulated rainfall amount between January 1 and October 10, 2022, on the occurrence of landslides, averaging out the effects of the other predictors. The orange lines indicate the occurrences of landslides. b) Effect of hillslope gradient, c) of lithozone, and d) road widening.
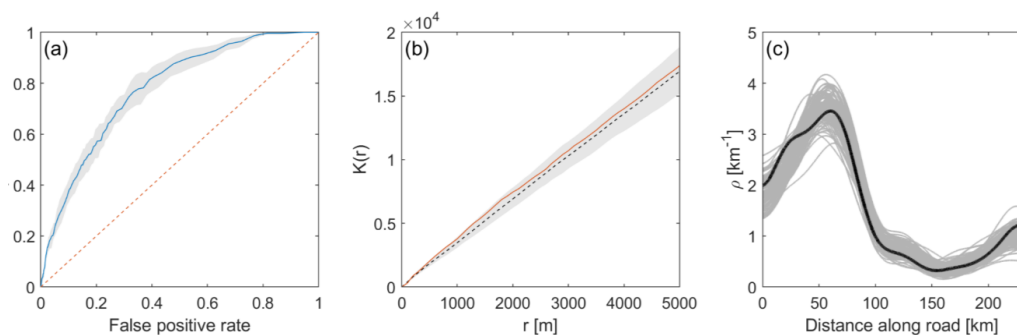
Figure 7: Evaluation of the loglinear model including rainfall, slope, lithozones and road widening. a) Receiver-operating-characteristics (ROC) curve. The area-under-the-curve (AUC) metric is 0.77. b) The inhomogeneous K-function corrects for the influence of an inhomogeneous Poisson point process model and tests for second order effects (e.g., spatial clustering). Acceptance intervals of a theoretical model without point independence are shown in gray. The red line is the empirical inhomogeneous K-function, which indicates clustering. c) Comparison of observed landslide densities (black line) with densities obtained from 100 random realizations (gray lines) from the model.
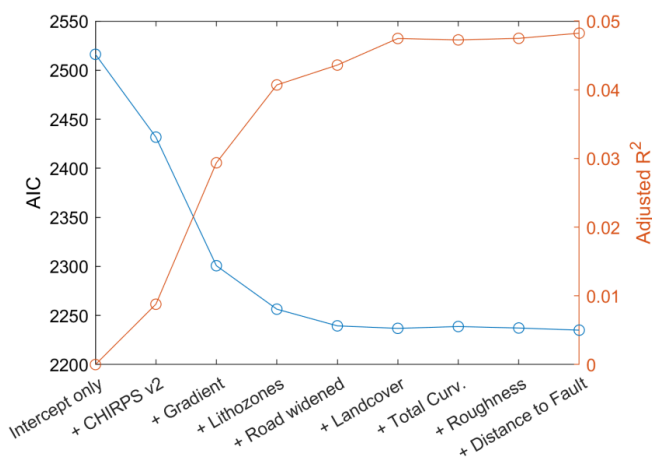
Figure 8: Forward stepwise selection of additional explanatory covariates in the loglinear model of road-blocking landslides.

Tables

Table 1. Overview of the rainfall products.

Product	Full form	Spatial resolution	Link to source	Reference
IMD1	Indian Meteorological Department 1	0.25° x 0.25°	https://www.imdpune.gov.in/cmpg/Griddata/Rainfall_25_Bin.html	Pai et al., 2014
IMD2	Indian Meteorological Department 2	0.25° x 0.25°	https://www.imdpune.gov.in/cmpg/Realtimedata/gpm/Rain_Download.html	Mitra et al., 2009
MSWEP v2	Multi-Source Weighted-Ensemble Precipitation	0.1° x 0.1°	http://www.gloh2o.org/	Beck et al., 2017
CHIRPS v2	Climate Hazards group Infrared Precipitation with Stations	0.05° x 0.05°	ftp://chg-ftpout.geog.ucsb.edu/pub/org/chg/products/CHIRPS-2.0/	Funk et al., 2015
IMERG late run	Integrated Multi-satellitE Retrievals for GPM	0.1° x 0.1°	https://gpm1.gesdisc.eosdis.nasa.gov/data/GPM_L3/GPM_3IMERGDL.06/	Huffman et al., 2019

635

Table 2. Definition of lithozones.

Lithozone	Aggregated lithologies	Id	Percentage of road

Id			
1	limestone, dolomitic limestone with shale	2072	
	shale with lenticles of limestone	2073	
	argillaceous limestone and clay	2074	17 %
	limestone, dolomite, shale, carb. phyllite/slate	2480	
	limestone	2457	
	dolomite	2456	
2	shale, quartzite, limestone and conglomerate	2109	
	phyllite, qtz, shale, dolomite, tuff with dolerite	2108	
	splintery shale with nodular limestone	746	
	massive sandy limestone	1799	33 %
	limestone, dolomite, shale and cherty quartzite	2482	
	quartzite, slate, lensoidal limestone and tuff	2486	
	massive sandy limestone	1799	
3	quartzite, limestone and occasional conglomerate	1943	
	quartzite, siltstone, chert and phosphatic shale	1944	6 %
	diamictite, quartzite, slate and boulder bed	2081	
	carbonaceous shale, slate, greywacke	2078	
4	quartzite and slate with basic metavolcanics	2464	
	basic meta-volcanics	2458	30 %
	basic / intermediate intrusive	2453	
	porphyritic nonfoliated granite	2452	
5	sericite quartz schist, chlorite schist	2463	
	chlorite schist, hornblende-albite-zoisite schist	2461	
	phyllite with chloritic, graphitic & carbonaceous	2462	
	schist, augen gneiss, quartzite & amphibolite	3702	
	quartz-sericite-chlorite schist & limestone	3701	14 %
	schist, gneiss, marble and basic intrusives	3747	
	gneiss, kyanite schist, quartzite, calc-silicate	3752	
	quartzite and quartz mica schist	3744	
	calc silicate, quartzite, schist, marble band	3743	

[a]Id refers to the UID given in the original data (Geological Survey of India, 2022)

640 **Table 3.** Aggregation of land cover classes derived from the Copernicus Global Land Service version 3 Globe 2015-2019. Remaining map codes in the original data were not concerned along the NH-7.

Aggregated land cover class	Map codes
Closed forest	111-116
Open forest	121-126

Shrubland	20, 30
Cropland	40
Built-up	50